

## Article

# Fine Aerosol Acidity and Water during Summer in the Eastern North Atlantic

Theodora Nah<sup>1,2,\*</sup> , Junwei Yang<sup>1</sup>, Jian Wang<sup>3</sup>, Amy P. Sullivan<sup>4</sup> and Rodney J. Weber<sup>5</sup>

<sup>1</sup> School of Energy and Environment, City University of Hong Kong, Hong Kong, China; jwyang6-c@my.cityu.edu.hk

<sup>2</sup> State Key Laboratory of Marine Pollution, City University of Hong Kong, Hong Kong, China

<sup>3</sup> Department of Energy, Environmental and Chemical Engineering, Washington University in St. Louis, Saint Louis, MO 63130, USA; jian@wustl.edu

<sup>4</sup> Department of Atmospheric Science, Colorado State University, Fort Collins, CO 80523, USA; amy.sullivan@colostate.edu

<sup>5</sup> School of Earth and Atmospheric Sciences, Georgia Institute of Technology, Atlanta, GA 30332, USA; rweber@eas.gatech.edu

\* Correspondence: theodora.nah@cityu.edu.hk; Tel.: +852-3442-5578

**Abstract:** Aerosol pH governs many important atmospheric processes that occur in the marine boundary layer, including regulating halogen and sulfur chemistries, and nutrient fertilization of surface ocean waters. In this study, we investigated the acidity of PM<sub>1</sub> over the eastern North Atlantic during the Aerosol and Cloud Experiments in Eastern North Atlantic (ACE-ENA) aircraft campaign. The ISORROPIA-II thermodynamic model was used to predict PM<sub>1</sub> pH and water. We first investigated the sensitivities of PM<sub>1</sub> pH and water predictions to gas-phase NH<sub>3</sub> and HNO<sub>3</sub> concentrations. Our sensitivity analysis indicated that even though NH<sub>3</sub> and HNO<sub>3</sub> were present at very low concentrations in the eastern North Atlantic during the campaign, PM<sub>1</sub> pH calculations can still be sensitive to NH<sub>3</sub> concentrations. Specifically, NH<sub>3</sub> was needed to constrain the pH of populations of PM<sub>1</sub> that had low mass concentrations of NH<sub>4</sub><sup>+</sup> and non-volatile cations (NVCs). We next assumed that gas-phase NH<sub>3</sub> and HNO<sub>3</sub> concentrations during the campaign were 0.15 and 0.09 μg m<sup>-3</sup>, respectively, based on previous measurements conducted in the eastern North Atlantic. Using the assumption that PM<sub>1</sub> were internally mixed (i.e., bulk PM<sub>1</sub>), we determined that PM<sub>1</sub> pH ranged from 0.3–8.6, with a mean pH of 5.0 ± 2.3. The pH depended on both  $H_{air}^+$  and  $W_i$ .  $H_{air}^+$  was controlled primarily by the NVCs/SO<sub>4</sub><sup>2-</sup> molar ratio, while  $W_i$  was controlled by the SO<sub>4</sub><sup>2-</sup> mass concentration and RH. Changes in pH with altitude were driven primarily by changes in SO<sub>4</sub><sup>2-</sup>. Since aerosols in marine atmospheres are rarely internally mixed, the scenario where non-sea salt species and sea-salt species were present in two separate aerosol modes in the PM<sub>1</sub> (i.e., completely externally mixed) was also considered. Smaller pH values were predicted for the aerosol mode comprised only of non-sea salt species compared to the bulk PM<sub>1</sub> (difference of around 1 unit on average). This was due to the exclusion of sea-salt species (especially hygroscopic alkaline NVCs) in this aerosol mode, which led to increases in  $H_{air}^+$  values and decreases in  $W_i$  values. This result demonstrated that assumptions of aerosol mixing states can impact aerosol pH predictions substantially, which will have important implications for evaluating the nature and magnitude of pH-dependent atmospheric processes that occur in the marine boundary layer.

**Keywords:** aerosol water; aerosol pH; aqueous phase; remote marine boundary layer; non-volatile cations



**Citation:** Nah, T.; Yang, J.; Wang, J.; Sullivan, A.P.; Weber, R.J. Fine Aerosol Acidity and Water during Summer in the Eastern North Atlantic. *Atmosphere* **2021**, *12*, 1040. <https://doi.org/10.3390/atmos12081040>

Academic Editor: Mikhail Arshinov

Received: 12 July 2021

Accepted: 12 August 2021

Published: 13 August 2021

**Publisher's Note:** MDPI stays neutral with regard to jurisdictional claims in published maps and institutional affiliations.



**Copyright:** © 2021 by the authors. Licensee MDPI, Basel, Switzerland. This article is an open access article distributed under the terms and conditions of the Creative Commons Attribution (CC BY) license (<https://creativecommons.org/licenses/by/4.0/>).

## 1. Introduction

Aerosol acidity is an important property that governs many atmospheric processes that transform the mass concentration and composition of atmospheric aerosols, which in turn have important implications for air quality, climate, and human and ecosystem health. Examples of these atmospheric processes include enhancing the formation of

secondary organic aerosols (SOA) through acid-catalyzed reactions during the oxidation of volatile organic compounds (VOCs) [1–3], controlling the gas-aerosol partitioning of atmospheric semi-volatile basic and acidic species (e.g., ammonia (NH<sub>3</sub>), hydrochloric acid (HCl), nitric acid (HNO<sub>3</sub>)) [4–6], regulating the water solubilities of trace metals and nutrient species in aerosols [7–9], and modulating halogen and sulfur chemistries in the marine boundary layer [10,11]. pH is the parameter commonly used to characterize the acidity of atmospheric aerosols. Aerosol pH is defined as the negative logarithm of the molality-based hydronium ion (H<sub>3</sub>O<sup>+</sup>) activity in the aerosol aqueous phase [12]. Water-soluble ions play important roles in affecting aerosol acidity because they control the balance of ions in the aerosol aqueous phase and regulate the water uptake properties (i.e., hygroscopicity) of aerosols. Water-soluble inorganic ions can comprise a substantial fraction of the dry aerosol mass (25% to 75%), with the main components typically being ammonium (NH<sub>4</sub><sup>+</sup>), sulfate (SO<sub>4</sub><sup>2-</sup>), and nitrate (NO<sub>3</sub><sup>-</sup>) [13]. Depending on the location, significant mass concentrations of chloride (Cl<sup>-</sup>) and non-volatile cations (NVCs) such as sodium (Na<sup>+</sup>), calcium (Ca<sup>2+</sup>), potassium (K<sup>+</sup>), and magnesium (Mg<sup>2+</sup>) can also be present in atmospheric aerosols. This is especially the case for aerosols found in marine atmospheres and/or areas affected by severe dust events [14]. Fresh dust and sea salts are naturally alkaline due to the presence of inorganic carbonates [11]. However, dust and sea salts can become acidified during atmospheric aging due to the uptake of acidic gases (e.g., HNO<sub>3</sub>) [15–17]. The mixing characteristics of dust and sea salts within the aerosol will also change during atmospheric aging. For example, NaCl in fresh sea salts are typically capped by small quantities of other inorganic species, whereas aged sea salts can be completely encased within large quantities of other inorganic and organic species [18]. NVCs are usually present in larger concentrations in PM<sub>2.5</sub> than in PM<sub>1</sub>, which results in PM<sub>2.5</sub> typically being less acidic than PM<sub>1</sub> [7]. Water-soluble organic species present in the aerosol can also impact the aerosol pH by changing the H<sub>3</sub>O<sup>+</sup> activity in the aqueous phase and/or by diluting the aqueous phase with aerosol water associated with the organic fraction. However, Battaglia Jr. et al. (2019) showed that water-soluble inorganic ions alone adequately constrain the aerosol pH under conditions where liquid–liquid phase separation is not expected to occur [19].

Due to the complex physicochemical properties of atmospheric aerosols, there are few analytical methods that can directly measure the pH of atmospheric aerosols [14,20]. Thermodynamic equilibrium models (e.g., E-AIM [21], ISORROPIA-II [22], EQUISOLV II [23]) currently provide the most reliable estimates of aerosol pH. Thermodynamic equilibrium models calculate the aerosol water content and pH based on model inputs of meteorological data, gas and aerosol measurements [14]. All particle-phase species are assumed to be internally mixed within the aerosol, so one value of pH represents the aerosol population. PM<sub>1</sub> NH<sub>4</sub><sup>+</sup>, SO<sub>4</sub><sup>2-</sup>, and NO<sub>3</sub><sup>-</sup> ions are usually measured in ambient studies, thus their concentrations are often included in thermodynamic calculations of aerosol pH and water. In contrast, the concentrations of Cl<sup>-</sup> and NVCs are sometimes excluded from thermodynamic calculations since they are seldom included in aerosol composition measurements [24]. This is due, in part, to the small contributions of these species to the overall aerosol mass in most locations. The omission of NVCs from thermodynamic calculations can result in erroneously predicted aerosol ammonium-to-sulfate (NH<sub>4</sub><sup>+</sup>/SO<sub>4</sub><sup>2-</sup>) molar ratios and pH. Using datasets from southeastern USA during the SOAS campaign and from northeastern USA during the WINTER campaign, Guo et al. (2018) showed that the omission of NVCs in ISORROPIA-II calculations resulted in the overprediction of NH<sub>4</sub><sup>+</sup>/SO<sub>4</sub><sup>2-</sup> molar ratios in fine aerosols [25]. This was due to NH<sub>4</sub><sup>+</sup> ions replacing the excluded NVCs in the thermodynamic calculations. The aerosol pH values for the SOAS and WINTER field campaigns only increased by 0.1 to 0.5 units when NVCs were included in thermodynamic calculations. However, this small increase in aerosol pH values can affect the predicted gas-aerosol partitioning of semi-volatile species (e.g., NH<sub>4</sub><sup>+</sup>–NH<sub>3</sub>, NO<sub>3</sub><sup>-</sup>–HNO<sub>3</sub>, Cl<sup>-</sup>–HCl) due to their nonlinear sensitivity to aerosol pH [5,6]. It should be noted that the concentrations of NVCs in the SOAS and WINTER

datasets were very low (i.e., close to or below the limits of detection of aerosol composition measurements) compared to the concentrations of  $\text{NH}_4^+$ ,  $\text{SO}_4^{2-}$ , and  $\text{NO}_3^-$  ions. It is likely that aerosol pH will only be insensitive to the model exclusion of NVCs in datasets from environments where NVC concentrations are low.

Previous studies have shown that gas-phase  $\text{NH}_3$  measurements serve as important constraints on aerosol pH in thermodynamic calculations of aerosols in populated continental locations with anthropogenic emissions of  $\text{NH}_3$  from agriculture, traffic, and industry [26,27]. This is because not including gas-phase  $\text{NH}_3$  concentrations in thermodynamic calculations can result in pH predictions that are too low since the thermodynamic model will partition a fraction of the particle-phase  $\text{NH}_4^+$  to the gas phase to make up for the missing gas-phase  $\text{NH}_3$ , which will result in a prediction of a more acidic aerosol. However,  $\text{NH}_3$  is not commonly measured in field campaigns, especially in studies that are held in remote marine locations [28]. Satellite observations and model simulations have shown that outside of polluted air masses originating from continental and/or biomass burning regions,  $\text{NH}_3$  mixing ratios over the Atlantic and Pacific Oceans are typically in the parts per trillion (ppt) range [28,29]. This is in line with previous  $\text{NH}_3$  measurements conducted over the northeast Atlantic Ocean during the ASTEX/MAGE campaign where the measured  $\text{NH}_3$  mixing ratios ranged from <25 ppt to 710 ppt [30]. The low  $\text{NH}_3$  concentrations in remote marine regions is attributed to low oceanic  $\text{NH}_x$  emissions and the short lifetime of  $\text{NH}_3$  [28,31–33]. Thus,  $\text{NH}_3$  concentrations in remote marine locations are substantially lower than those in continental locations. Given that alkaline NVCs are expected to comprise a significant mass fraction of aerosols in remote marine atmospheres, it is currently unclear whether  $\text{NH}_3$  is an important neutralizing agent of  $\text{PM}_{10}$  acidity and/or serves as a key constraint on aerosol pH in thermodynamic calculations of aerosols in remote marine atmospheres.

The acidity of aerosols in environments with intensive anthropogenic activities have received the most attention. Pye et al. (2020) compiled these studies and reported that the mean pH of fine aerosols ranged from around 1 to 6 [14].  $\text{NH}_4^+$ ,  $\text{SO}_4^{2-}$ , and  $\text{NO}_3^-$  ions are the dominant water-soluble inorganic ions in fine aerosols in most areas with intensive anthropogenic activities; thus, aerosol pH and water are usually regulated by these three ions in these environments. Locations with very high levels of acidic sulfate (e.g., southeastern USA, southeast Asia) had fine aerosol pH values of less than 2 [14,34,35]. Higher  $\text{PM}_{2.5}$  pH values (around 2 to 3) were reported for Los Angeles during the CalNex campaign due to higher aerosol water concentrations, which was a result of higher total  $\text{NO}_3^-$  concentrations and  $\text{NO}_3^-$ – $\text{HNO}_3$  partitioning [5]. Locations close to areas with intensive agricultural activities that emitted high levels of  $\text{NH}_3$  (e.g., parts of mainland China and Europe) had fine pH values as high as 6 [14,36,37]. Higher fine aerosol pH values (around 4 to 6) were reported for urban areas impacted by sea salt (e.g., San Paulo, Hawaii) and dust (e.g., Inner Mongolia, Po Valley) due to the neutralizing effect of NVCs [14,38–41].

There have been comparatively few studies on the acidity of aerosols in remote marine atmospheres. Keene and Savoie (1998) used a Cl phase partitioning model to estimate that aerosols had pH values ranging from the mid-2s to the mid-3s at Bermuda under moderately polluted conditions [42]. Fridlind and Jacobson (2000) applied the EQISOLV II thermodynamic model to estimate that aerosols over the minimally polluted Southern Ocean had pH values that ranged from 0 to 5 [4]. The acidic nature of aerosols observed in these studies were explained by the rapid titration of fresh sea salt alkalinity by acids scavenged from the gas phase or formed via chemical reactions occurring within the aerosol [4,43,44]. Recently, Nault et al. (2021) used the E-AIM thermodynamic model to estimate that  $\text{PM}_{10}$  over the Pacific, Southern, Atlantic, and Arctic Oceans had pH values ranging from –1 to 3 [28]. It should be noted that NVCs were excluded from thermodynamic calculations performed by Nault et al. (2021), and this resulted in lower estimated aerosol pH values compared to estimates that included accumulation-mode NVCs in thermodynamic calculations. Given the important role that aerosol acidity plays in many atmospheric processes that occur in the remote marine boundary layer (e.g., halogen and

sulfur chemistries), it is important to have a strong understanding of the factors that control aerosol pH and water (e.g., roles of  $\text{NH}_3$  and NVCs, aerosol mixing characteristics) in different remote marine atmospheres.

In this paper, we used the  $\text{PM}_{10}$  dataset obtained with a particle-into-liquid sampler (PILS) during the summer 2017 flights of the Aerosol and Cloud Experiments in Eastern North Atlantic (ACE-ENA) campaign to characterize the acidity of  $\text{PM}_{10}$  over the eastern North Atlantic. Measurements were carried out in the Azores archipelago in the eastern North Atlantic during the ACE-ENA campaign [45]. Although the ACE-ENA campaign had two intense operating periods (IOP) that occurred during summer 2017 (June to July) and winter 2018 (January to February), the  $\text{PM}_{10}$  dataset obtained during the winter IOP was not used because the mass concentrations of many water-soluble aerosol constituents essential for aerosol acidity predictions were very low (i.e., close to or below the limits of detection of aerosol composition measurements). The composition and properties of aerosols in the eastern North Atlantic are known to be influenced by a variety of natural processes, including sea spray aerosol production, the entrainment of aerosols from the free troposphere, new particle formation, and the processing of aerosols inside and outside of clouds [46–48]. Aerosols in the eastern North Atlantic are also subjected to occasional anthropogenic influences caused by local pollution from the Azorean islands and polluted air masses originating from North America and northern Europe [30,46–51]. These factors make the eastern North Atlantic an ideal location for investigations of pH and water content of  $\text{PM}_{10}$  in a remote marine environment where anthropogenic influences are minor. Since each flight consisted of different vertical profiles, we will also provide insights into how  $\text{PM}_{10}$  acidity changes with altitude in the eastern North Atlantic.

## 2. Materials and Methods

The ACE-ENA campaign was a multi-investigator study that included measurements onboard the DOE G-1 research aircraft [45]. The G-1 was operated out of the Lajes airport on Terceira Island. A total of 20 flights occurred during the summer IOP. Each flight comprised of four to six vertical profiles, which allowed measurements as a function of altitude to be obtained. The payload onboard the G-1 included instruments used to measure meteorological parameters, trace gases, aerosols, and cloud properties. Details about the flight paths and the list of instruments onboard the G-1 can be found in Zawadowicz et al. (2021) and Wang et al. (2021) [46,47].

### 2.1. PILS Sampling and Offline Ion Chromatography Analysis

A PILS was used to measure the water-soluble ions in  $\text{PM}_{10}$ . The PILS is an aerosol collection device that continuously collects ambient aerosols into water [52,53]. In the PILS, aerosols were mixed with water vapor at around 100 °C produced from heated ultrapure deionized water. The resulting droplets were impacted onto a plate, thus providing a liquid sample with aerosols dissolved in it. During each flight, the PILS continuously sampled from an isokinetic inlet at a flowrate of 15 L/min. The size-cut was provided by a non-rotating MOUDI impactor with 50% transmission efficiency of 1  $\mu\text{m}$  (aerodynamic diameter) at 1 atm ambient pressure [54]. Upstream of the PILS were two honeycomb denuders coated with sodium carbonate and phosphorous acid to remove acidic and basic gases, respectively. The PILS was connected to a Bretchel fraction collector to collect liquid samples for offline ion chromatography (IC) analysis [53]. The liquid sample was pushed into the fraction collector vials at a flowrate of 0.65 mL/min by a peristaltic pump to collect ~1.2 mL of sample per vial every 2 min. The fraction collector system holds 721.5 mL polypropylene vials (Microsolv Technology Corporation, Leland, NC, USA) per carousel. During each flight, carousels were pre-loaded and manually switched out once all the vials in that carousel had been filled. Blank samples were also collected on each flight by diverting the sampled air through a High Efficiency Particulate-Free Air (HEPA) filter (Pall Corp., Port Washington, NY, USA) before being introduced into the PILS. All the data were background corrected. After each flight, all the vials were removed from the carousels

and capped with solid caps (Microsolv Technology Corporation, Leland, NC, USA). The capped vials were stored refrigerated until analyzed. IC analysis of the samples began in the field and were completed back at Colorado State University (CSU) following the end of the intensive.

Each vial was brought back to room temperature and then analyzed for anions and cations. For each analysis, 300  $\mu\text{L}$  aliquots were transferred to polypropylene vials. Anions were measured using a potassium hydroxide gradient provided by an eluent generator at a flowrate of 0.015 mL/min. The complete run time was 65 min with an injection volume of 35  $\mu\text{L}$ . The cations were determined using a Dionex DX-500 IC with a gradient pump, conductivity detector, and self-regenerating cation suppressor. A Dionex CS-12A analytical column (3 mm  $\times$  150 mm) using an eluent of 20 mM methanesulfonic acid at a flowrate of 0.5 mL/min was used. The injection volume and run time were 190  $\mu\text{L}$  and 17 min, respectively. In the discussions presented below, we focused on  $\text{PM}_1$   $\text{NH}_4^+$ ,  $\text{SO}_4^{2-}$ ,  $\text{NO}_3^-$ ,  $\text{Cl}^-$ ,  $\text{Na}^+$ ,  $\text{Ca}^{2+}$ ,  $\text{K}^+$ , and  $\text{Mg}^{2+}$  inorganic ions measured by the PILS-fraction collector system.

## 2.2. Thermodynamic Calculations

The thermodynamic equilibrium model ISORROPIA-II was used to determine the equilibrium phase-partitioning and composition of an  $\text{NH}_4^+$ - $\text{SO}_4^{2-}$ - $\text{NO}_3^-$ - $\text{Cl}^-$ - $\text{Na}^+$ - $\text{Ca}^{2+}$ - $\text{K}^+$ - $\text{Mg}^{2+}$ -water aerosol [22]. The aerosol pH calculated in this study used the molal definition consistent with the  $\text{pH}_F$  definition by Pye et al. (2020) [14]:

$$\text{pH} = -\log_{10} \frac{1000H_{air}^+}{W} \cong -\log_{10} \frac{1000H_{air}^+}{W_i} \quad (1)$$

where  $H_{air}^+$  ( $\mu\text{g m}^{-3}$ ) is the hydronium ion concentration per volume of air, and  $W$  ( $\mu\text{g m}^{-3}$ ) is the bulk aerosol water concentration. For simplicity,  $\text{H}_3\text{O}^+$  is denoted here as  $\text{H}^+$  even though we acknowledge that the unhydrated hydrogen ion is rare in aqueous solutions.  $W$  is the sum of the bulk aerosol water concentrations associated with inorganic and organic species (i.e.,  $W = W_i + W_o$ ). The concentrations of organic species were low during the summer IOP [47], thus we expect  $W_o$  to be low. Previous studies have also shown that the effects of  $W_o$  to the aerosol pH is not significant [19,34]. Thus, we report aerosol pH only considering  $W_i$ .  $W_i$  and  $H_{air}^+$  are outputs of the ISORROPIA-II model.

ISORROPIA-II was run in “forward” mode based on the assumptions that the aerosol was internally mixed, that it existed in a “metastable” equilibrium state (i.e., the aerosols only existed in liquid form), and that the aerosol was in thermodynamic equilibrium with the gas phase. Discussions about how the assumption of aerosols being internally mixed affects predictions of aerosol pH and water will be presented below. In “forward” mode, the model uses the input of the total concentration of a species (i.e., gas + particle) to calculate the gas-aerosol equilibrium partitioning concentrations. The water-soluble inorganic  $\text{NH}_4^+$ ,  $\text{SO}_4^{2-}$ ,  $\text{NO}_3^-$ ,  $\text{Cl}^-$ ,  $\text{Na}^+$ ,  $\text{Ca}^{2+}$ ,  $\text{K}^+$ , and  $\text{Mg}^{2+}$  concentrations measured by the PILS-fraction collector system and the meteorological parameters measured onboard the G-1 were used as model inputs. Gas-phase inorganic measurements were not available for the ACE-ENA campaign. Thus, we used gas-phase  $\text{NH}_3$  and  $\text{HNO}_3$  concentrations previously measured in the eastern North Atlantic in our thermodynamic calculations [30]. Discussions about how the inclusions of gas-phase  $\text{NH}_3$  and  $\text{HNO}_3$  concentrations in the thermodynamic calculations impact the predictions of aerosol pH and water will be presented below. In “reverse” mode, the model uses the input of only the particle-phase concentration of a species to calculate the gas-aerosol equilibrium partitioning concentrations. “Reverse” mode was not used in this study because this mode is known to be very sensitive to measurement errors, which can cause large errors in the predicted aerosol pH [55].

## 3. Results and Discussion

Conditions in the eastern North Atlantic were clean during the summer IOP. Zawadowicz et al. (2021), reported that the mass concentrations of non-refractory  $\text{PM}_1$

organics,  $\text{NH}_4^+$ ,  $\text{SO}_4^{2-}$ , and  $\text{NO}_3^-$  measured by an Aerodyne High-Resolution Time-of-Flight Aerosol Mass Spectrometer during the summer IOP were low, with the mean mass concentrations of these species ranging from 0.01–0.55  $\mu\text{g m}^{-3}$  [47]. Low mass concentrations of water-soluble inorganic species were also measured by the PILS-fraction collector system (Table S1). These low mass concentrations were unsurprising since the sampling area was far from anthropogenic pollution sources. This provided us with an ideal opportunity to investigate  $\text{PM}_1$  pH and water in a clean marine environment where anthropogenic influences were minor.

Thermodynamic calculations were performed for periods where the RH was between 35% and 95%. Periods where the RH was below 35% were excluded because the aerosols were less likely to be in a liquid state, which would lead to high uncertainties in pH predictions due to uncertain activity coefficients associated with highly concentrated solutions under these low RH conditions [56–58]. Periods where the RH was above 95% were also excluded because the exponential growth in aerosol water with RH would introduce large pH uncertainties [58]. We used the mass concentrations of water-soluble  $\text{PM}_1$   $\text{NH}_4^+$ ,  $\text{SO}_4^{2-}$ ,  $\text{NO}_3^-$ ,  $\text{Cl}^-$ ,  $\text{Na}^+$ ,  $\text{Ca}^{2+}$ ,  $\text{K}^+$ , and  $\text{Mg}^{2+}$  measured by the PILS-fraction collector system. For the dataset used for the thermodynamic calculations, NVCs (i.e.,  $\text{Na}^+$ ,  $\text{Ca}^{2+}$ ,  $\text{K}^+$ , and  $\text{Mg}^{2+}$ ) comprised  $36.3 \pm 16.6\%$  of the  $\text{PM}_1$  inorganic mass concentration (which we defined here as the sum of  $\text{NH}_4^+$ ,  $\text{SO}_4^{2-}$ ,  $\text{NO}_3^-$ ,  $\text{Cl}^-$ ,  $\text{Na}^+$ ,  $\text{Ca}^{2+}$ ,  $\text{K}^+$ , and  $\text{Mg}^{2+}$  mass concentrations). However, there were time periods where NVCs comprised less than 20% of the  $\text{PM}_1$  inorganic mass concentration.

In the first part of this paper, we assumed that all the water-soluble inorganic ions were internally mixed in the aerosol, and explored the sensitivity of  $\text{PM}_1$  pH and water to gas-phase  $\text{NH}_3$  and  $\text{HNO}_3$  concentrations (Section 3.1), and the key factors that strongly influenced predictions of  $\text{PM}_1$  pH and water (Section 3.2). In the second part of this paper, we investigated how assumptions regarding how sea salt species and NVCs mixed in aerosols (i.e., internal vs. external mixtures) will impact predictions of  $\text{PM}_1$  pH and water (Section 3.3).

### 3.1. Sensitivity of $\text{PM}_1$ pH and Water to the Inclusion of Gas-Phase $\text{NH}_3$ and $\text{HNO}_3$ Concentrations to ISORROPIA-II

Murphy et al. (2017) previously showed that gas-phase  $\text{NH}_3$  and  $\text{HNO}_3$  measurements can serve as important constraints on aerosol pH in thermodynamic calculations of aerosols in populated continental locations with anthropogenic emissions [26]. Gas-phase inorganic measurements were not available for the ACE-ENA campaign. However, gas-phase measurements conducted several years ago during the ASTEX/MAGE study indicated that  $\text{NH}_3$  and  $\text{HNO}_3$  concentrations are usually low in the eastern North Atlantic during the summer. During the ASTEX/MAGE study,  $\text{NH}_3$  mixing ratios ranged from <25 ppt to 710 ppt with a study-averaged mixing ratio of around 200 ppt (around  $0.15 \mu\text{g m}^{-3}$ ), while  $\text{HNO}_3$  mixing ratios ranged from <8 ppt to 164 ppt with a study-averaged mixing ratio of around 28 ppt (around  $0.09 \mu\text{g m}^{-3}$ ) [30]. In this section, we explore the sensitivities of  $\text{PM}_1$  pH and water predictions to gas-phase  $\text{NH}_3$  and  $\text{HNO}_3$  concentrations. This will allow us to determine the effects of excluding gas-phase  $\text{NH}_3$  and  $\text{HNO}_3$  concentrations in aerosol pH calculations for clean remote environments that have substantially lower concentrations of gas-phase  $\text{NH}_3$  and  $\text{HNO}_3$  compared to populated continental locations. The sensitivities were assessed by perturbing the ISORROPIA-II input concentrations of total ammonium ( $\text{TA} = \text{NH}_3 + \text{NH}_4^+$ ) and total nitrate ( $\text{TN} = \text{HNO}_3 + \text{NO}_3^-$ ). Different concentrations of  $\text{NH}_3$  and  $\text{HNO}_3$  were added into the system, and the responses in  $\text{PM}_1$  pH and water were quantified. The overall goal of these sensitivity tests is to determine the conditions where gas-phase  $\text{NH}_3$  and  $\text{HNO}_3$  serve as critical constraints on aerosol pH in thermodynamic calculations of aerosols measured during the ACE-ENA campaign.

In our  $\text{NH}_3$  sensitivity analysis, we added 0.01, 0.12, 0.15, and  $0.29 \mu\text{g m}^{-3}$  of  $\text{NH}_3$  into the system. The median and mean  $\text{NH}_3$  concentrations measured during the ASTEX/MAGE study were 0.12 and  $0.15 \mu\text{g m}^{-3}$ , respectively [30]. The addition of 0.12 and

$0.15 \mu\text{g m}^{-3}$  of  $\text{NH}_3$  into the system resulted in average  $\text{NH}_3/\text{TA}$  mass ratios of  $0.61 \pm 0.18$  and  $0.65 \pm 0.17$ , respectively. It was determined that 0.01 and  $0.29 \mu\text{g m}^{-3}$  were the 25th and 75th percentile  $\text{NH}_3$  concentrations measured during the ASTEX/MAGE study, respectively [30]. The addition of 0.01 and  $0.29 \mu\text{g m}^{-3}$  of  $\text{NH}_3$  into the system resulted in average  $\text{NH}_3/\text{TA}$  mass ratios of  $0.16 \pm 0.14$  and  $0.77 \pm 0.13$ , respectively. Based on the average  $\text{NH}_3/\text{TA}$  mass ratios, the addition of  $0.01 \mu\text{g m}^{-3}$  of  $\text{NH}_3$  into the system assumes that majority of the TA species is in the aerosol phase in the form of  $\text{NH}_4^+$  ions. In contrast, the addition of 0.12, 0.15, and  $0.29 \mu\text{g m}^{-3}$  of  $\text{NH}_3$  into the system assumes that the majority of the TA species is in the gas phase as  $\text{NH}_3$ . Figure 1a compares the different median and mean pH values with the 10th, 25th, 75th, and 90th percentile values calculated for the different  $\text{NH}_3$  concentrations added into the system. The median pH did not change substantially for the range of  $\text{NH}_3$  concentrations added (differed by a maximum of 0.05 units). However, the mean pH increased by approximately 0.4 units upon the addition of  $\geq 0.12 \mu\text{g m}^{-3}$  of  $\text{NH}_3$  into the system. In addition, the 10th percentile pH value increased by approximately 1.8 units when  $\geq 0.12 \mu\text{g m}^{-3}$  of  $\text{NH}_3$  was added. This was because a subset of  $\text{PM}_{10}$  in the dataset had low mass concentrations of  $\text{NH}_4^+$  and NVCs. The addition of  $0.12 \mu\text{g m}^{-3}$  of  $\text{NH}_3$  into the system resulted in a decrease in  $H_{\text{air}}^+$  for this subset of  $\text{PM}_{10}$  due to  $\text{NH}_3\text{-NH}_4^+$  gas-aerosol partitioning. This was demonstrated by the noticeable decrease in the 10th percentile  $H_{\text{air}}^+$  value ( $1.7 \times 10^{-4} \mu\text{g m}^{-3}$  to  $3.2 \times 10^{-5} \mu\text{g m}^{-3}$ ) when  $0.12 \mu\text{g m}^{-3}$  of  $\text{NH}_3$  was added into the system (Figure S1a). Adding more  $\text{NH}_3$  into the system did not change the pH of this subset of  $\text{PM}_{10}$  substantially, as demonstrated by the somewhat similar mean pH values (differed by a maximum of 0.1 units) and 10th percentile pH values (differed by a maximum of 0.2 units) obtained when 0.12 vs. 0.15 and  $0.29 \mu\text{g m}^{-3}$  of  $\text{NH}_3$  were added into the system. This was because aerosol pH was weakly sensitive to a wide  $\text{NH}_3$  concentration range due to pH buffering caused by the partitioning of  $\text{NH}_3$  between the gas and aerosol phases [59]. The addition of 0.01 to  $0.29 \mu\text{g m}^{-3}$  of  $\text{NH}_3$  into the system did not result in significant changes in  $W_i$  (Figure S1b).

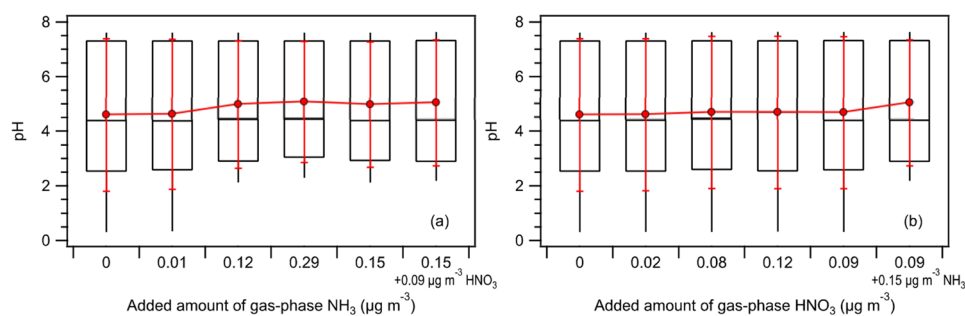


**Figure 1.** Box plots depicting the median pH values calculated by ISORROPIA-II for the different concentrations of gas-phase (a)  $\text{NH}_3$ , and (b)  $\text{HNO}_3$  added into the system. Standard box-and-whisker plots are shown, with the 90th and 10th percentile data indicated by black error bars. The top and bottom of the box are the interquartile ranges (75th and 25th percentile) centered around the median value (50th percentile). The red symbols denote the means, and the red error bars are 1 standard deviation.

In our  $\text{HNO}_3$  sensitivity analysis, we added 0.02, 0.08, 0.09, and  $0.12 \mu\text{g m}^{-3}$  of  $\text{HNO}_3$  into the system. The median and mean  $\text{HNO}_3$  concentrations measured during the ASTEX/MAGE study were 0.08 and  $0.09 \mu\text{g m}^{-3}$ , respectively [30]. The addition of 0.08 and  $0.09 \mu\text{g m}^{-3}$  of  $\text{HNO}_3$  into the system resulted in average  $\text{HNO}_3/\text{TN}$  mass ratios of  $0.75 \pm 0.15$  and  $0.77 \pm 0.14$ , respectively. It was determined that 0.02 and  $0.12 \mu\text{g m}^{-3}$  were the 25th and 75th percentile  $\text{HNO}_3$  concentrations measured during the ASTEX/MAGE study, respectively [30]. The addition of 0.02 and  $0.12 \mu\text{g m}^{-3}$  of  $\text{HNO}_3$  into the system resulted in average  $\text{HNO}_3/\text{TN}$  mass ratios of  $0.48 \pm 0.19$  and  $0.81 \pm 0.12$ , respectively. Figure 1b compares the different median and mean pH values with the 10th, 25th, 75th,

and 90th percentile values calculated for the different HNO<sub>3</sub> concentrations added into the system. Unlike the addition of NH<sub>3</sub> into the system, adding HNO<sub>3</sub> into the system did not lead to noticeable changes in the calculated pH values. After the addition of up to 0.12 µg m<sup>-3</sup> of HNO<sub>3</sub> into the system, the median and mean pH values only differed by 0.29 and 0.1 units, respectively. These small changes in the pH values were due to the weak sensitivities of  $H_{air}^+$  and  $W_i$  to the range of HNO<sub>3</sub> concentrations added into the system. There were no significant changes in  $H_{air}^+$ , while the median and mean  $W_i$  values only increased by a maximum of 0.22 and 0.25 µg m<sup>-3</sup>, respectively (Figure S2). The increase in  $W_i$  can be attributed to the thermodynamic model partitioning a fraction of HNO<sub>3</sub> from the gas phase to the aerosol phase, and the hygroscopicity of particle-phase NO<sub>3</sub><sup>-</sup> salts.

Overall, our sensitivity analysis demonstrated that even though NH<sub>3</sub> (and HNO<sub>3</sub>) may be present at very low concentrations in clean marine atmospheres (relative to continental locations with anthropogenic emissions), aerosol pH calculations will be sensitive to NH<sub>3</sub> concentrations under some conditions. This will especially be the case for populations of aerosols that have low mass concentrations of NVCs where TA will act as the main neutralizing agent of aerosol acidity. For pH predictions of PM<sub>1</sub> during the summer IOP, we observed that not including NH<sub>3</sub> concentrations into TA in aerosol pH calculations will lead to the overestimation of aerosol acidity for populations of aerosols that have low mass concentrations of NH<sub>4</sub><sup>+</sup> and NVCs. This is because NH<sub>3</sub>-NH<sub>4</sub><sup>+</sup> gas-aerosol partitioning calculated in thermodynamic models will be derived solely on the measured particle-phase NH<sub>4</sub><sup>+</sup> mass concentrations. A fraction of this NH<sub>4</sub><sup>+</sup> will be partitioned into the gas phase as NH<sub>3</sub> in the thermodynamic model, thus leading to the release of more particle-phase H<sup>+</sup>, which will result in the prediction of a more acidic aerosol. In this study, for PM<sub>1</sub> populations with low mass concentrations of NH<sub>4</sub><sup>+</sup> and NVCs, adding 0.15 µg m<sup>-3</sup> of NH<sub>3</sub> into the system generally resulted in the predicted pH increasing by approximately 2 units. Hence, NH<sub>3</sub> measurements can serve as important constraints on the pH of aerosols found in clean marine atmospheres.

### 3.2. Factors That Influence PM<sub>1</sub> pH and Water

For the rest of the discussion carried out in this paper, we assumed that gas-phase NH<sub>3</sub> and HNO<sub>3</sub> concentrations during the summer IOP were 0.15 and 0.09 µg m<sup>-3</sup>, respectively [30]. These were the mean concentrations measured during the ASTEX/MAGE study. Under these conditions, the predicted PM<sub>1</sub> pH ranged from 0.3 to 8.6, with a mean pH of 5.0 ± 2.3. Figure 1 shows the different median and mean pH values with the 10th, 25th, 75th, and 90th percentile values calculated when 0.15 µg m<sup>-3</sup> of NH<sub>3</sub> and 0.09 µg m<sup>-3</sup> of HNO<sub>3</sub> were included in the thermodynamic calculations.

The dependence of PM<sub>1</sub> pH on  $H_{air}^+$  is shown in Figure 2. An increase in  $H_{air}^+$  generally led to a noticeable decrease in PM<sub>1</sub> pH.  $H_{air}^+$  was observed to depend mainly on the total molar concentration of NVCs (i.e., NVCs = Na<sup>+</sup> + Ca<sup>2+</sup> + K<sup>+</sup> + Mg<sup>2+</sup>) relative to the SO<sub>4</sub><sup>2-</sup> molar concentration in the aerosol. The  $H_{air}^+$  values were grouped based on their NVCs/SO<sub>4</sub><sup>2-</sup> molar ratios, and their statistics are shown as a function of the NVCs/SO<sub>4</sub><sup>2-</sup> molar ratio in Figure 3.  $H_{air}^+$  decreased substantially when the NVCs/SO<sub>4</sub><sup>2-</sup> molar ratio increased from 0 to 3. In addition, when the amount of SO<sub>4</sub><sup>2-</sup> was low, even small amounts of NVCs impacted  $H_{air}^+$  significantly. However, when the amount of SO<sub>4</sub><sup>2-</sup> was high (comprised at least 30% of the mole fraction of the sum of PM<sub>1</sub> NH<sub>4</sub><sup>+</sup>, SO<sub>4</sub><sup>2-</sup>, NO<sub>3</sub><sup>-</sup>, Cl<sup>-</sup>, Na<sup>+</sup>, Ca<sup>2+</sup>, K<sup>+</sup>, and Mg<sup>2+</sup>), small amounts of the NVCs (up to 30% of the mole fraction of the sum of PM<sub>1</sub> NH<sub>4</sub><sup>+</sup>, SO<sub>4</sub><sup>2-</sup>, NO<sub>3</sub><sup>-</sup>, Cl<sup>-</sup>, Na<sup>+</sup>, Ca<sup>2+</sup>, K<sup>+</sup>, and Mg<sup>2+</sup>) did not reduce  $H_{air}^+$  substantially. Previous studies have reported that the pH of aerosols in other marine and coastal regions was similarly impacted by the NVCs/SO<sub>4</sub><sup>2-</sup> molar ratio. During the WINTER campaign, the aerosol pH increased by more than 2 units when the SO<sub>4</sub><sup>2-</sup> mass concentration decreased and the NaCl mass concentration increased during flights made over or near coastal regions in northeastern USA [6]. Fine aerosols over the Southern Ocean became less acidic when the Na<sup>+</sup>/SO<sub>4</sub><sup>2-</sup> ratio increased [4]. The relationship between aerosol acidity and the NVCs/SO<sub>4</sub><sup>2-</sup> molar ratio can be explained by the non-volatile

nature of alkaline NVCs present in aerosols. The NVCs preferentially and irreversibly neutralized  $\text{SO}_4^{2-}$  in the aerosol over  $\text{NH}_3$ , which reduced the concentration of  $\text{H}^+$  in the aerosol.

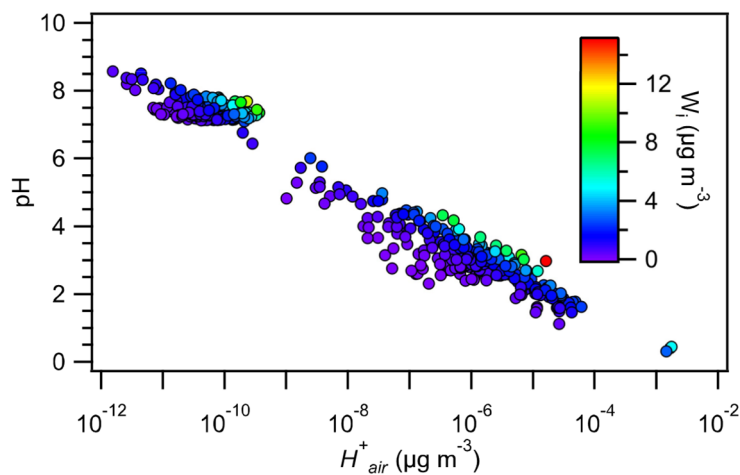


**Figure 2.**  $\text{PM}_1$  pH versus  $H_{air}^+$  colored by  $W_i$ . Gas-phase  $\text{NH}_3$  and  $\text{HNO}_3$  concentrations were assumed to be  $0.15$  and  $0.09 \mu\text{g m}^{-3}$ , respectively, in the ISORROPIA-II calculations.

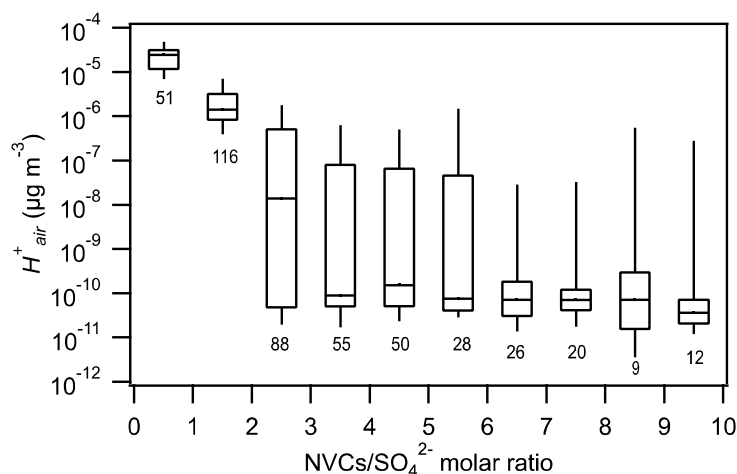


**Figure 3.** Box plot of  $H_{air}^+$  versus the  $\text{NVCs}/\text{SO}_4^{2-}$  molar ratio. The box plot was generated by segregating the data into ten equally-spaced  $\text{NVCs}/\text{SO}_4^{2-}$  molar ratio bins. Standard box-and-whisker plots are shown, with the 90th and 10th percentile data indicated by black error bars. The top and bottom of the box are the interquartile ranges (75th and 25th percentile) centered around the median value (50th percentile). The number of points considered for each bin are also shown.

The influence of  $W_i$  on  $\text{PM}_1$  pH was also evident in Figure 2. For any given  $H_{air}^+$  value, smaller pH values were predicted for smaller  $W_i$  values. Since  $W_i$  was predicted by ISORROPIA-II from the mass concentrations of water-soluble inorganic species, one would expect  $W_i$  to be dependent on RH and the mass concentrations of hygroscopic inorganic species. Although NVCs are known hygroscopic species that can elevate  $W_i$ , no obvious relationship was observed between the NVCs mass loadings and  $W_i$  for  $\text{PM}_1$ .  $\text{SO}_4^{2-}$  was the major anion species with high hygroscopicity in  $\text{PM}_1$ . In general,  $W_i$  increased with the  $\text{SO}_4^{2-}$  mass concentration and RH (Figure S3). No obvious relationships were observed between  $W_i$  and  $\text{NO}_3^-$  and  $\text{Cl}^-$ , and this was likely due to the low mass concentrations of  $\text{NO}_3^-$  and  $\text{Cl}^-$ .

To determine the major factors that influence  $\text{PM}_1$  pH during the summer IOP, we performed a series of sensitivity tests of  $\text{PM}_1$  pH to major water-soluble inorganic ions (i.e.,

$\text{SO}_4^{2-}$ ,  $\text{Na}^+$ ,  $\text{Ca}^{2+}$ ,  $\text{K}^+$ , and  $\text{Mg}^{2+}$ ), ( $\text{TA} = \text{NH}_3 + \text{NH}_4^+$ ), and meteorological conditions (i.e., RH and temperature). In each sensitivity test, we evaluated how the variable affected the  $\text{PM}_{10}$  pH by inputting the real-time measured value of this variable and the mean values of the other parameters into ISORROPIA-II. The relative standard deviation (RSD) of the re-calculated pH values reflected the degree of sensitivity that variations in the variable had on aerosol acidity. The larger the RSD was, the greater the impact the variable had on the aerosol acidity (and vice versa). This method was previously utilized by Ding et al. (2019) and Wang et al. (2020) to determine the major factors that influence aerosol pH in different parts of China [36,60].

Table 1 shows the results of the  $\text{PM}_{10}$  pH sensitivity tests.  $\text{PM}_{10}$  pH was found to be most sensitive to  $\text{SO}_4^{2-}$  and  $\text{Ca}^{2+}$ . Elevated  $\text{SO}_4^{2-}$  levels were essential for the increase of  $H_{air}^+$  and  $W_i$  (Table S2), thus it played a key role in influencing aerosol acidity. Elevated  $\text{Ca}^{2+}$  levels could reduce  $H_{air}^+$  substantially to increase the  $\text{PM}_{10}$  pH (Table S2), especially in cases where the mass concentration of  $\text{SO}_4^{2-}$  in the aerosol was low. In the ISORROPIA-II output,  $\text{Ca}^{2+}$  existed primarily as  $\text{CaSO}_4$ , which is a marginally water-soluble species [22].  $\text{PM}_{10}$  pH was insensitive to variations in TA, and this could be due to the high mean values of NVCs used in the sensitivity test. As discussed in Section 3.1, variations in TA will mostly affect the pH of  $\text{PM}_{10}$  populations that have low mass concentrations of NVCs. Although  $\text{PM}_{10}$  pH was somewhat insensitive to variations in meteorological conditions (i.e., RH and temperature), RH impacted  $W_i$  substantially (Table S2). Elevated RH conditions could enhance water uptake, which will lead to an increase in  $W_i$  (Figure S3). Consequently, high levels of  $W_i$  can promote the gas-to-aerosol partitioning of  $\text{NH}_3$  and  $\text{HNO}_3$ .

**Table 1.** Sensitivity of  $\text{PM}_{10}$  pH to  $\text{SO}_4^{2-}$ , TA ( $\text{NH}_3 + \text{NH}_4^+$ ),  $\text{Na}^+$ ,  $\text{Ca}^{2+}$ ,  $\text{K}^+$ ,  $\text{Mg}^{2+}$ , RH, and temperature. The larger the relative standard deviation (RSD) was, the greater the impact the variable had on pH.

Impact Factor	$\text{SO}_4^{2-}$	TA	$\text{Na}^+$	$\text{Ca}^{2+}$	$\text{K}^+$	$\text{Mg}^{2+}$	RH	Temp
pH-RSD (%)	33.4	0.12	11.9	35.6	12.9	24.6	1.8	0.6

Figure 4a shows the vertical distribution of  $\text{PM}_{10}$  pH from 0 to 2500 m altitude. The majority of the  $\text{PM}_{10}$  pH values reported here were for  $\text{PM}_{10}$  below 1 km due to the RH range (35–95%) chosen for thermodynamic calculations. RH, temperature, and aerosol mass concentrations decreased with altitude. The 250 m altitude-binned statistics showed a somewhat uniform  $\text{PM}_{10}$  pH range of 2 to 7.5 for altitudes below 1.5 km, and slightly lower  $\text{PM}_{10}$  pH ranges for altitudes above 1.5 km. The 250 m altitude-binned median and mean  $\text{PM}_{10}$  pH values increased with altitude. This can be attributed primarily to the decrease in  $H_{air}^+$  with altitude, which was likely caused by the decrease in the molar ratio of  $\text{SO}_4^{2-}$  with altitude (Figure 4b). Here, we defined the  $\text{SO}_4^{2-}$  molar ratio as the  $\text{SO}_4^{2-}$  molar concentration divided by the sum of the molar concentrations of  $\text{PM}_{10}$   $\text{NH}_4^+$ ,  $\text{SO}_4^{2-}$ ,  $\text{NO}_3^-$ ,  $\text{Cl}^-$ ,  $\text{Na}^+$ ,  $\text{Ca}^{2+}$ ,  $\text{K}^+$ , and  $\text{Mg}^{2+}$ .

Crustals were treated explicitly in our above ISORROPIA-II analysis. Previous studies that used the E-AIM thermodynamic model to predict aerosol acidity sometimes treated crustals as mole-equivalent  $\text{Na}^+$  (i.e.,  $\text{Ca}^{2+} = 2\text{Na}^+$ ,  $\text{Mg}^{2+} = 2\text{Na}^+$ , and  $\text{K}^+ = \text{Na}^+$ ) because E-AIM cannot explicitly treat crustal species. The mole-equivalent  $\text{Na}^+$  treatment does not impact aerosol pH predictions significantly (difference of less than 1 unit) in areas with low levels of NVCs. We examined the impact that treating crustals as mole-equivalent  $\text{Na}^+$  will have on pH predictions of ACE-ENA  $\text{PM}_{10}$  where NVC concentrations were substantial. Higher mean and median pH values were predicted (approximately 1.0 units and 3.1 units higher, respectively) when  $\text{Ca}^{2+}$ ,  $\text{Mg}^{2+}$ , and  $\text{K}^+$  were treated as mole-equivalent  $\text{Na}^+$  (Figure S4). Differences in the predicted pH values were due to substantial differences in predicted  $H_{air}^+$  and  $W_i$  values between the two treatments, which were caused by the non-ideality of divalent ions (i.e.,  $\text{Ca}^{2+}$  and  $\text{Mg}^{2+}$ ) and the different hygroscopicity behaviors of  $\text{Na}^+$  salts vs.  $\text{Ca}^{2+}$ ,  $\text{Mg}^{2+}$ , and  $\text{K}^+$  salts. In particular,  $W_i$  values were noticeably higher

in the mole-equivalent  $\text{Na}^+$  treatment (approximately  $1.0 \mu\text{g m}^{-3}$  higher on average). This was due to the formation of marginally soluble  $\text{CaSO}_4$  in calculations where crustals were explicitly treated [22].  $\text{CaSO}_4$  does not significantly contribute to water uptake [56], which will lead to smaller predicted  $W_i$  values in these calculations. Overall, our analysis emphasizes the need to treat crustals explicitly in thermodynamic calculations of  $\text{PM}_{10}$  in marine atmospheres (or any other environments with substantial mass concentrations of NVCs). Not doing so will lead to erroneous predictions of aerosol pH, which has important implications for gas-aerosol partitioning predictions.

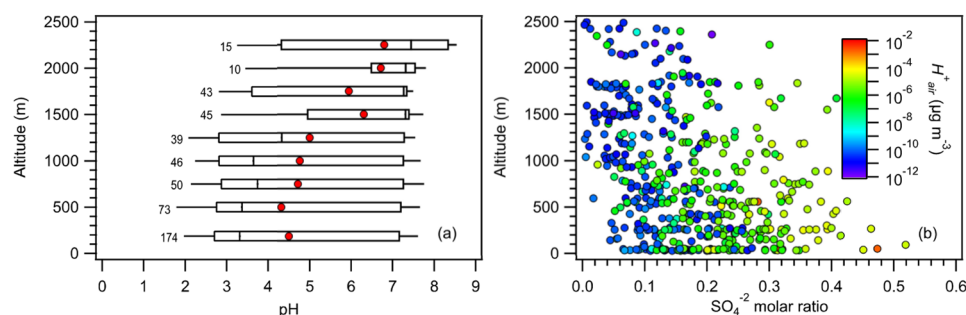


**Figure 4.** (a) Vertical profile of  $\text{PM}_{10}$  pH (250 m altitude-binned) from 0 to 2500 m altitude. Standard box-and-whisker plots are shown, with the 90th and 10th percentile data indicated by black error bars. The top and bottom of the box are the interquartile ranges (75th and 25th percentile) centered around the median value (50th percentile). The red symbols denote mean pH values. The number of points considered for each bin are also shown. (b) Vertical profile of the  $\text{SO}_4^{2-}$  molar ratio (colored by  $H_{air}^+$ ).

### 3.3. Internal Mixture vs. Mixture with Two Modes

Our analysis up to this point assumed that all the water-soluble inorganic ions were internally mixed in the aerosol. Thus, pH predictions presented above were obtained using the total  $\text{PM}_{10}$   $\text{NH}_4^+$ ,  $\text{SO}_4^{2-}$ ,  $\text{NO}_3^-$ ,  $\text{Cl}^-$ ,  $\text{Na}^+$ ,  $\text{Ca}^{2+}$ ,  $\text{K}^+$ , and  $\text{Mg}^{2+}$  mass concentrations measured by the PILS-fraction collector system for thermodynamic calculations. However, aerosols that are close to source regions are likely externally mixed. Gas-aerosol interactions, interactions between particle-phase species, and atmospheric aging during transport will make aerosols more homogeneous, eventually leading to internally mixed aerosols [61]. Particle-phase species in marine atmospheres have traditionally been divided into two groups: those that originate from sea salt, and those that originate from non-sea salt (nss) sources. In relatively clean marine atmospheres like the eastern North Atlantic, sea-salt species (especially the NVCs) are expected to contribute a significant mass fraction of aerosols. Sea salts are known to be naturally alkaline [11]. In addition, sea salts are mainly present in the coarse mode, with a tail extending into the fine mode [62]. Hence, non-sea salt species are often not well mixed with sea-salt species in fine aerosols due to their different sources and sizes.

In this section, we investigate how assumptions regarding how sea-salt species and NVCs were mixed in aerosols (i.e., internal vs. external mixtures) will impact predictions of  $\text{PM}_{10}$  pH and water. We consider the scenario that non-sea salt species and sea-salt species were present in two separate aerosol modes in the  $\text{PM}_{10}$  (i.e., completely externally mixed). The mode consisting of non-sea salt species was assumed to be internally mixed. Again, we assumed that gas-phase  $\text{NH}_3$  and  $\text{HNO}_3$  concentrations were  $0.15$  and  $0.09 \mu\text{g m}^{-3}$ , respectively.  $\text{NH}_3$ ,  $\text{HNO}_3$ , and water vapor were assumed to still equilibrate between these two modes due to the short equilibrating timescales for  $\text{PM}_{10}$  [56,63,64]. Assuming that all the measured  $\text{Na}^+$  and  $\text{Cl}^-$  in  $\text{PM}_{10}$  were exclusively from sea salt, mass concentrations of non-sea salt  $\text{K}^+$ ,  $\text{Mg}^{2+}$ ,  $\text{Ca}^{2+}$ , and  $\text{SO}_4^{2-}$  can be calculated using the following equations [65]:

$$\text{nssK}^+ = \text{K}^+ - 0.037 \times \text{Na}^+ \quad (2)$$

$$nssMg^{2+} = Mg^{2+} - 0.012 \times Na^+ \quad (3)$$

$$nssCa^{2+} = Ca^{2+} - 0.037 \times Na^+ \quad (4)$$

$$nssSO_4^{2-} = SO_4^{2-} - 0.25 \times Na^+ \quad (5)$$

For instances where the calculated mass concentration of the non-sea salt species were a negative value, the negative calculated value was substituted with  $0 \mu\text{g m}^{-3}$ . This treatment of negative calculated non-sea salt mass concentrations only affected 2% of the dataset. Non-sea salt NVCs comprised  $28.9\% \pm 15.9\%$  of the  $PM_{10}$  non-sea salt inorganic mass concentration. Thermodynamic calculations were performed to predict the pH of the aerosol mode containing non-sea salt species. These results were then compared to those presented in Section 3.2, which provided insights into how the assumption that non-sea salt species are internally mixed with sea-salt species in the aerosol will impact pH predictions.

Figure 5 compares the median and mean pH values with the 10th, 25th, 75th, and 90th percentile values calculated for internally mixed aerosols vs. the aerosol mode containing only non-sea salt species. For the aerosol mode comprised only of non-sea salt species, ISORROPIA-II predicted smaller median and mean pH values compared to those predicted using the internally mixed aerosol assumption (differed by 1.8 and 0.8 units, respectively). The differences in the predicted pH values were due to substantial differences in predicted  $H_{air}^+$  and  $W_i$  values (Figure S5). On average, higher  $H_{air}^+$  values were predicted for the aerosol mode containing only non-sea salt species compared to internally mixed aerosols ( $3.20 \times 10^{-5}$  vs.  $1.23 \times 10^{-5} \mu\text{g m}^{-3}$ ). This was unsurprising since the aerosol mode containing only non-sea salt species had lower mass concentrations of alkaline NVCs after the exclusion of sea-salt NVCs in the thermodynamic calculations. In addition, smaller  $W_i$  values were predicted for the aerosol mode containing only non-sea salt species ( $1.7$  vs.  $0.9 \mu\text{g m}^{-3}$ ) due to the lower mass concentrations of hygroscopic NVC species.

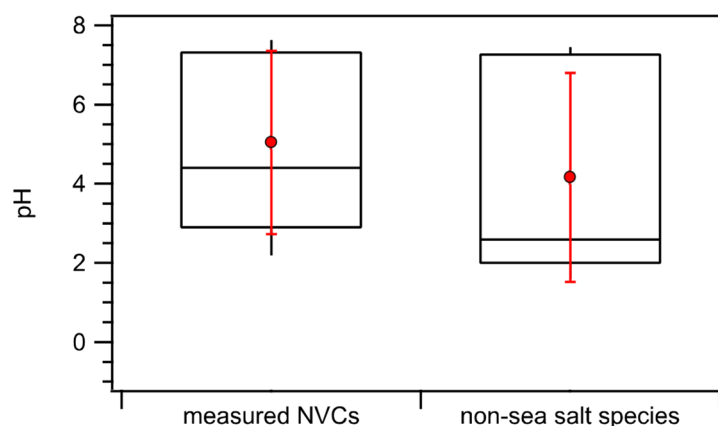


**Figure 5.** Box plots depicting the median pH values calculated by ISORROPIA-II for internally mixed aerosols vs. the aerosol mode containing only non-sea salt species. Standard box-and-whisker plots are shown, with the 90th and 10th percentile data indicated by black error bars. The top and bottom of the box are the interquartile ranges (75th and 25th percentile) centered around the median value (50th percentile). The red symbols denote the means, and the red error bars are 1 standard deviation.

It should be noted that the range of predicted pH values for the aerosol mode containing only non-sea salt species was higher than those reported by Nault et al. for  $PM_{10}$  over the Pacific, Southern, Atlantic, and Arctic Oceans (pH 1–3) [28]. This was because Nault et al. (2021) excluded all the NVCs (i.e., non-sea salt NVCs and sea-salt NVCs) from their thermodynamic calculations. The authors showed that  $PM_{10}$  NVC mass concentrations were low during their field campaign, and thus would not impact their  $PM_{10}$  pH predictions substantially. In contrast, we observed that the non-sea salt NVCs constituted a significant mass fraction of the  $PM_{10}$  non-sea salt inorganic mass concentration during the

ACE-ENA campaign (an average of  $28.9\% \pm 15.9\%$ ), and thus they were included in our thermodynamic calculations for the aerosol mode containing only non-sea salt species.

Overall, our results showed that assumptions of the mixing characteristics of aerosols (i.e., internally vs. externally mixed) can significantly impact predicted pH values for fine aerosols in marine atmospheres. Despite these differences, the pH values of the aerosol mode containing only non-sea salt species demonstrated similar trends as those of the internally mixed aerosols. The pH of the aerosol mode containing only non-sea salt species depended strongly on  $H_{air}^+$ , where an increase in  $H_{air}^+$  generally led to a noticeable decrease in pH. Similarly,  $H_{air}^+$  was observed to depend mainly on the total molar concentration of non-sea salt NVCs relative to the molar concentration of non-sea salt  $SO_4^{2-}$  in the aerosol mode. In addition, the pH values of the aerosol mode containing only non-sea salt species also increased with altitude due to the decrease in the molar ratio of non-sea salt  $SO_4^{2-}$  in the aerosol mode (i.e., non-sea salt  $SO_4^{2-}$  molar concentration divided by the sum of the molar concentrations of non-sea salt species) with altitude.

#### 4. Conclusions

The pH of aerosols in remote marine atmospheres influences many important atmospheric processes that occur in the marine boundary layer, including regulating halogen and sulfur chemistries, and nutrient fertilization of surface ocean waters [11,14]. However, the scarcity and limitations (e.g., use of ion balance and molar ratio to determine aerosol pH) of currently available data of aerosol acidity in remote marine atmospheres hinders our understanding of these processes. In this study, we used ISORROPIA-II to predict the acidity of  $PM_{10}$  over the eastern North Atlantic during the summer IOP of the ACE-ENA campaign. Conditions over the eastern North Atlantic were clean during the summer IOP, as reflected by the low mass concentrations of water-soluble species in  $PM_{10}$  measured by the PILS-fraction collector system. We first assessed the sensitivities of  $PM_{10}$  pH and water predictions to a range of gas-phase  $NH_3$  and  $HNO_3$  concentrations. Our sensitivity analysis revealed that aerosol pH calculations are sensitive to  $NH_3$  concentrations even though  $NH_3$  may be present at very low concentrations in clean marine atmospheres. Not including  $NH_3$  concentrations in aerosol pH calculations will lead to the overestimation of aerosol acidity for populations of aerosols that have low mass concentrations of  $NH_4^+$  and NVCs. Thus,  $NH_3$  measurements serve as important constraints on pH calculations of aerosols in clean marine atmospheres.

Gas-phase  $NH_3$  and  $HNO_3$  concentrations measured previously in the eastern North Atlantic were used to constrain the aerosol pH calculations. Using the assumption that aerosols were internally mixed (i.e., bulk  $PM_{10}$ ), we determined that  $PM_{10}$  pH ranged from 0.3 to 8.6, with a mean pH of  $5.0 \pm 2.3$ . The pH depended on both  $H_{air}^+$  and  $W_i$ .  $H_{air}^+$  was controlled primarily by the total molar concentration of NVCs relative to the  $SO_4^{2-}$  molar concentration, while  $W_i$  was controlled by the  $SO_4^{2-}$  mass concentration and RH. Overall, the pH was most sensitive to changes in  $PM_{10}$   $SO_4^{2-}$  and  $Ca^{2+}$  mass concentrations. Elevated  $SO_4^{2-}$  levels were essential for the increase of  $H_{air}^+$  and  $W_i$ . Elevated  $Ca^{2+}$  levels could lead to substantial reduction of  $H_{air}^+$ , especially in cases where the mass concentration of  $SO_4^{2-}$  in the aerosol was low. Our analysis also indicated that  $PM_{10}$  acidity decreased with altitude. This was due to the decrease in  $H_{air}^+$  with altitude, which was likely caused by the decrease in the molar ratio of acidic  $SO_4^{2-}$  with altitude.

Since aerosols in marine atmospheres are rarely internally mixed, we also considered the scenario where non-sea salt species and sea-salt species were present in two separate aerosol modes (i.e., completely externally mixed) in the  $PM_{10}$ . We showed that smaller pH values would be predicted for the aerosol mode comprised only of non-sea salt species (difference of around 1 unit on average). This was due to the exclusion of sea-salt species (especially hygroscopic alkaline NVCs), which generally led to increases in  $H_{air}^+$  values and decreases in  $W_i$  values. This analysis indicated that assumptions of aerosol mixing states can impact aerosol pH predictions substantially. Given the non-linear response of many marine boundary layer atmospheric processes to aerosol pH, further assessment

of the possible effects of aerosol mixing states on aerosol pH should be carried out for other marine atmospheres that are chemically different from the eastern North Atlantic conditions evaluated in this study.

**Supplementary Materials:** The following are available online at <https://www.mdpi.com/article/10.3390/atmos12081040/s1>. Figure S1: Box plots depicting the median (a)  $H_{air}^+$ , and (b)  $W_i$  values calculated by ISORROPIA-II for the different concentrations of gas-phase  $NH_3$  added into the system. Figure S2: Box plots depicting the median (a)  $H_{air}^+$ , and (b)  $W_i$  values calculated by ISORROPIA-II for the different concentrations of gas-phase  $HNO_3$  added into the system. Figure S3: Box plots of  $W_i$  vs. (a)  $SO_4^{2-}$ , and (b) RH. Figure S4: Box plots depicting the median (a) pH, (b)  $H_{air}^+$ , and (c)  $W_i$  values calculated by ISORROPIA-II where crustals were treated explicitly vs. as mole-equivalent  $Na^+$ . Figure S5: Box plots depicting the median (a)  $H_{air}^+$ , and (b)  $W_i$  values calculated by ISORROPIA-II for internally mixed aerosols vs. the aerosol mode containing only non-sea salt species. Table S1: Average mass concentrations of chemical species measured by the PILS-fraction collector system. Table S2: Sensitivity of  $H_{air}^+$  and  $W_i$  to  $SO_4^{2-}$ , TA ( $NH_3 + NH_4^+$ ),  $Na^+$ ,  $Ca^{2+}$ ,  $K^+$ ,  $Mg^{2+}$ , RH, and temperature.

**Author Contributions:** Data curation: A.P.S. and R.J.W.; formal analysis and investigation: J.Y. and T.N.; writing—original draft: T.N.; writing—review and editing: T.N., J.Y., J.W., R.J.W. and A.P.S. All authors have read and agreed to the published version of the manuscript.

**Funding:** T.N. and J.Y. were supported by startup funds from the City University of Hong Kong (project number 9610409). J.W. was supported by the Atmospheric System Research (ASR) program as part of the DOE Office of Biological and Environmental Research under awards No. DE-SC0020259. A.P.S. and R.J.W. were supported by the Department of Energy (DOE) under contract DOE 333890.

**Institutional Review Board Statement:** Not applicable.

**Informed Consent Statement:** Not applicable.

**Data Availability Statement:** All datasets used in this paper are publicly available on the ARM website ([arm.gov/data](http://arm.gov/data), accessed on 12 August 2021).

**Acknowledgments:** The authors thank the G-1 flight and ground crews for supporting the ACE-ENA campaign.

**Conflicts of Interest:** The authors declare no conflict of interest.

## References

1. Eddingsaas, N.C.; VanderVelde, D.G.; Wennberg, P.O. Kinetics and Products of the Acid-Catalyzed Ring-Opening of Atmospherically Relevant Butyl Epoxy Alcohols. *J. Phys. Chem. A* **2010**, *114*, 8106–8113. [[CrossRef](#)] [[PubMed](#)]
2. Jang, M.S.; Czoschke, N.M.; Lee, S.; Kamens, R.M. Heterogeneous Atmospheric Aerosol Production by Acid-Catalyzed Particle-Phase Reactions. *Science* **2002**, *298*, 814–817. [[CrossRef](#)] [[PubMed](#)]
3. Surratt, J.D.; Chan, A.W.H.; Eddingsaas, N.C.; Chan, M.; Loza, C.L.; Kwan, A.J.; Hersey, S.P.; Flagan, R.C.; Wennberg, P.O.; Seinfeld, J.H. Reactive Intermediates Revealed in Secondary Organic Aerosol Formation from Isoprene. *Proc. Natl. Acad. Sci. USA* **2010**, *107*, 6640–6645. [[CrossRef](#)] [[PubMed](#)]
4. Fridlind, A.M.; Jacobson, M.Z. A Study of Gas-Aerosol Equilibrium and Aerosol pH in the Remote Marine Boundary Layer during the First Aerosol Characterization Experiment (ACE 1). *J. Geophys. Res. Atmos.* **2000**, *105*, 17325–17340. [[CrossRef](#)]
5. Guo, H.; Liu, J.; Froyd, K.D.; Roberts, J.M.; Veres, P.R.; Hayes, P.L.; Jimenez, J.L.; Nenes, A.; Weber, R.J. Fine Particle pH and Gas-Particle Phase Partitioning of Inorganic Species in Pasadena, California, during the 2010 CalNex Campaign. *Atmos. Chem. Phys.* **2017**, *17*, 5703–5719. [[CrossRef](#)]
6. Guo, H.; Sullivan, A.P.; Campuzano-Jost, P.; Schroder, J.C.; Lopez-Hilfiker, F.D.; Dibb, J.E.; Jimenez, J.L.; Thornton, J.A.; Brown, S.S.; Nenes, A.; et al. Fine Particle pH and the Partitioning of Nitric Acid during Winter in the Northeastern United States. *J. Geophys. Res. Atmos.* **2016**, *121*, 10355–10376. [[CrossRef](#)]
7. Fang, T.; Guo, H.; Zeng, L.; Verma, V.; Nenes, A.; Weber, R.J. Highly Acidic Ambient Particles, Soluble Metals, and Oxidative Potential: A Link between Sulfate and Aerosol Toxicity. *Environ. Sci. Technol.* **2017**, *51*, 2611–2620. [[CrossRef](#)]
8. Longo, A.F.; Feng, Y.; Lai, B.; Landing, W.M.; Shelley, R.U.; Nenes, A.; Mihalopoulos, N.; Violaki, K.; Ingall, E.D. Influence of Atmospheric Processes on the Solubility and Composition of Iron in Saharan Dust. *Environ. Sci. Technol.* **2016**, *50*, 6912–6920. [[CrossRef](#)]
9. Meskhidze, N.; Chameides, W.L.; Nenes, A.; Chen, G. Iron Mobilization in Mineral Dust: Can Anthropogenic  $SO_2$  Emissions Affect Ocean Productivity? *Geophys. Res. Lett.* **2003**, *30*. [[CrossRef](#)]

10. Katoshevski, D.; Nenes, A.; Seinfeld, J.H. A Study of Processes that Govern the Maintenance of Aerosols in the Marine Boundary Layer. *J. Aerosol Sci.* **1999**, *30*, 503–532. [[CrossRef](#)]
11. Keene, W.C.; Sander, R.; Pszenny, A.A.P.; Vogt, R.; Crutzen, P.J.; Galloway, J.N. Aerosol pH in the Marine Boundary Layer: A Review and Model Evaluation. *J. Aerosol Sci.* **1998**, *29*, 339–356. [[CrossRef](#)]
12. Buck, R.P.; Rondinini, S.; Covington, A.K.; Baucke, F.G.K.; Brett, C.M.A.; Camoes, M.F.; Milton, M.J.T.; Mussini, T.; Naumann, R.; Pratt, K.W.; et al. Measurement of pH. Definition, Standards, and Procedures. *Pure Appl. Chem.* **2002**, *74*, 2169–2200. [[CrossRef](#)]
13. Heintzenberg, J. Fine Particles in the Global Troposphere A Review. *Tellus Ser. B Chem. Phys. Meteorol.* **1989**, *41*, 149–160. [[CrossRef](#)]
14. Pye, H.O.T.; Nenes, A.; Alexander, B.; Ault, A.P.; Barth, M.C.; Clegg, S.L.; Collett, J.L.; Fahey, K.M.; Hennigan, C.J.; Herrmann, H.; et al. The Acidity of Atmospheric Particles and Clouds. *Atmos. Chem. Phys.* **2020**, *20*, 4809–4888. [[CrossRef](#)] [[PubMed](#)]
15. Bondy, A.L.; Wang, B.; Laskin, A.; Craig, R.L.; Nhliziyo, M.V.; Bertman, S.B.; Pratt, K.A.; Shepson, P.B.; Ault, A.P. Inland Sea Spray Aerosol Transport and Incomplete Chloride Depletion: Varying Degrees of Reactive Processing Observed during SOAS. *Environ. Sci. Technol.* **2017**, *51*, 9533–9542. [[CrossRef](#)]
16. Laskin, A.; Iedema, M.J.; Cowin, J.P. Quantitative Time-Resolved Monitoring of Nitrate Formation in Sea Salt Particles Using a CCSEM/EDX Single Particle Analysis. *Environ. Sci. Technol.* **2002**, *36*, 4948–4955. [[CrossRef](#)]
17. Laskin, A.; Moffet, R.C.; Gilles, M.K.; Fast, J.D.; Zaveri, R.A.; Wang, B.; Nigge, P.; Shutthanandan, J. Tropospheric Chemistry of Internally Mixed Sea Salt and Organic Particles: Surprising Reactivity of NaCl with Weak Organic Acids. *J. Geophys. Res. Atmos.* **2012**, *117*. [[CrossRef](#)]
18. Wang, H.; Wang, X.; Yang, X.; Li, W.; Xue, L.; Wang, T.; Chen, J.; Wang, W. Mixed Chloride Aerosols and their Atmospheric Implications: A Review. *Aerosol Air Qual. Res.* **2017**, *17*, 878–887. [[CrossRef](#)]
19. Battaglia, M.A., Jr.; Weber, R.J.; Nenes, A.; Hennigan, C.J. Effects of Water-Soluble Organic Carbon on Aerosol pH. *Atmos. Chem. Phys.* **2019**, *19*, 14607–14620. [[CrossRef](#)]
20. Freedman, M.A.; Ott, E.-J.E.; Marak, K.E. Role of pH in Aerosol Processes and Measurement Challenges. *J. Phys. Chem. A* **2019**, *123*, 1275–1284. [[CrossRef](#)] [[PubMed](#)]
21. Wexler, A.S.; Clegg, S.L. Atmospheric Aerosol Models for Systems Including the Ions  $H^+$ ,  $NH_4^+$ ,  $Na^+$ ,  $SO_4^{2-}$ ,  $NO_3^-$ ,  $Cl^-$ ,  $Br^-$ , and  $H_2O$ . *J. Geophys. Res. Atmos.* **2002**, *107*, ACH 14-11–ACH 14-14. [[CrossRef](#)]
22. Fountoukis, C.; Nenes, A. ISORROPIA II: A Computationally Efficient Thermodynamic Equilibrium Model for  $K^+$ - $Ca^{2+}$ - $Mg^{2+}$ - $NH_4^+$ - $Na^+$ - $SO_4^{2-}$ - $NO_3^-$ - $Cl^-$ - $H_2O$  Aerosols. *Atmos. Chem. Phys.* **2007**, *7*, 4639–4659. [[CrossRef](#)]
23. Jacobson, M.Z. *Fundamentals of Atmospheric Modeling*, 2nd ed.; Cambridge University Press: New York, NY, USA, 2005; p. 820.
24. Xu, J.; Song, S.; Harrison, R.M.; Song, C.; Wei, L.; Zhang, Q.; Sun, Y.; Lei, L.; Zhang, C.; Yao, X.; et al. An Interlaboratory Comparison of Aerosol Inorganic Ion Measurements by Ion Chromatography: Implications for Aerosol pH Estimate. *Atmos. Meas. Tech.* **2020**, *13*, 6325–6341. [[CrossRef](#)]
25. Guo, H.Y.; Nenes, A.; Weber, R.J. The Underappreciated Role of Nonvolatile Cations in Aerosol Ammonium-Sulfate Molar ratios. *Atmos. Chem. Phys.* **2018**, *18*, 17307–17323. [[CrossRef](#)]
26. Murphy, J.G.; Gregoire, P.K.; Tevlin, A.G.; Wentworth, G.R.; Ellis, R.A.; Markovic, M.Z.; VandenBoer, T.C. Observational Constraints on Particle Acidity using Measurements and Modelling of Particles and Gases. *Faraday Discuss.* **2017**, *200*, 379–395. [[CrossRef](#)] [[PubMed](#)]
27. Zheng, G.; Su, H.; Wang, S.; Andreae, M.O.; Pöschl, U.; Cheng, Y. Multiphase Buffer Theory Explains Contrasts in Atmospheric Aerosol Acidity. *Science* **2020**, *369*, 1374–1377. [[CrossRef](#)] [[PubMed](#)]
28. Nault, B.A.; Campuzano-Jost, P.; Day, D.A.; Jo, D.S.; Schroder, J.C.; Allen, H.M.; Bahreini, R.; Bian, H.; Blake, D.R.; Chin, M.; et al. Chemical Transport Models Often Underestimate Inorganic Aerosol Acidity in Remote Regions of the Atmosphere. *Commun. Earth Environ.* **2021**, *2*, 93. [[CrossRef](#)]
29. Bian, H.; Chin, M.; Hauglustaine, D.A.; Schulz, M.; Myhre, G.; Bauer, S.E.; Lund, M.T.; Karydis, V.A.; Kucsera, T.L.; Pan, X.; et al. Investigation of Global Particulate Nitrate from the AeroCom Phase III Experiment. *Atmos. Chem. Phys.* **2017**, *17*, 12911–12940. [[CrossRef](#)]
30. Huebert, B.J.; Zhuang, L.; Howell, S.; Noone, K.; Noone, B. Sulfate, Nitrate, Methane Sulfonate, Chloride, Ammonium, and Sodium Measurements from Ship, Island, and Aircraft During the Atlantic Stratocumulus Transition Experiment/Marine Aerosol Gas Exchange. *J. Geophys. Res. Atmos.* **1996**, *101*, 4413–4423. [[CrossRef](#)]
31. Paulot, F.; Jacob, D.J.; Johnson, M.T.; Bell, T.G.; Baker, A.R.; Keene, W.C.; Lima, I.D.; Doney, S.C.; Stock, C.A. Global Oceanic Emission of Ammonia: Constraints from Seawater and Atmospheric Observations. *Glob. Biogeochem. Cycles* **2015**, *29*, 1165–1178. [[CrossRef](#)]
32. Paulot, F.; Stock, C.; John, J.G.; Zadeh, N.; Horowitz, L.W. Ocean Ammonia Outgassing: Modulation by  $CO_2$  and Anthropogenic Nitrogen Deposition. *J. Adv. Modeling Earth Syst.* **2020**, *12*, e2019MS002026. [[CrossRef](#)]
33. Khan, M.A.H.; Lowe, D.; Derwent, R.G.; Foulds, A.; Chhantyal-Pun, R.; McFiggans, G.; Orr-Ewing, A.J.; Percival, C.J.; Shallcross, D.E. Global and Regional Model Simulations of Atmospheric Ammonia. *Atmos. Res.* **2020**, *234*, 104702. [[CrossRef](#)]
34. Guo, H.; Xu, L.; Bougiatioti, A.; Cerully, K.M.; Capps, S.L.; Hite, J.R., Jr.; Carlton, A.G.; Lee, S.H.; Bergin, M.H.; Ng, N.L.; et al. Fine-Particle Water and pH in the Southeastern United States. *Atmos. Chem. Phys.* **2015**, *15*, 5211–5228. [[CrossRef](#)]
35. Xue, J.; Lau, A.K.H.; Yu, J.Z. A Study of Acidity on  $PM_{2.5}$  in Hong Kong Using Online Ionic Chemical Composition Measurements. *Atmos. Environ.* **2011**, *45*, 7081–7088. [[CrossRef](#)]

36. Wang, S.B.; Wang, L.L.; Li, Y.Q.; Wang, C.; Wang, W.S.; Yin, S.S.; Zhang, R.Q. Effect of Ammonia on Fine-Particle pH in Agricultural Regions of China: Comparison between Urban and Rural Sites. *Atmos. Chem. Phys.* **2020**, *20*, 2719–2734. [[CrossRef](#)]
37. Kakavas, S.; Patoulias, D.; Zakoura, M.; Nenes, A.; Pandis, S.N. Size-Resolved Aerosol pH Over Europe During Summer. *Atmos. Chem. Phys.* **2021**, *21*, 799–811. [[CrossRef](#)]
38. Vieira-Filho, M.; Pedrotti, J.J.; Fornaro, A. Water-Soluble Ions Species of Size-Resolved Aerosols: Implications for the Atmospheric Acidity in Sao Paulo Megacity, Brazil. *Atmos. Res.* **2016**, *181*, 281–287. [[CrossRef](#)]
39. Pszenny, A.A.P.; Moldanov, J.; Keene, W.C.; Sander, R.; Maben, J.R.; Martinez, M.; Crutzen, P.J.; Perner, D.; Prinn, R.G. Halogen Cycling and Aerosol pH in the Hawaiian Marine Boundary Layer. *Atmos. Chem. Phys.* **2004**, *4*, 147–168. [[CrossRef](#)]
40. Wang, H.; Ding, J.; Xu, J.; Wen, J.; Han, J.; Wang, K.; Shi, G.; Feng, Y.; Ivey, C.E.; Wang, Y.; et al. Aerosols in an Arid Environment: The Role of Aerosol Water Content, Particulate Acidity, Precursors, and Relative Humidity on Secondary Inorganic Aerosols. *Sci. Total Environ.* **2019**, *646*, 564–572. [[CrossRef](#)] [[PubMed](#)]
41. Squizzato, S.; Masiol, M.; Brunelli, A.; Pistollato, S.; Tarabotti, E.; Rampazzo, G.; Pavoni, B. Factors Determining the Formation of Secondary Inorganic Aerosol: A Case Study in the Po Valley (Italy). *Atmos. Chem. Phys.* **2013**, *13*, 1927–1939. [[CrossRef](#)]
42. Keene, W.C.; Savoie, D.L. The pH of Deliquesced Sea-Salt Aerosol in Polluted Marine Air. *Geophys. Res. Lett.* **1998**, *25*, 2181–2184. [[CrossRef](#)]
43. Chameides, W.L.; Stelson, A.W. Aqueous-Phase Chemical Processes in Deliquescent Sea-Salt Aerosols: A Mechanism that Couples the Atmospheric Cycles of S and Sea Salt. *J. Geophys. Res. Atmos.* **1992**, *97*, 20565–20580. [[CrossRef](#)]
44. Erickson, D.J.; Seuzaret, C.; Keene, W.C.; Gong, S.L. A General Circulation Model Based Calculation of HCl and ClNO<sub>2</sub> Production from Sea Salt Dechlorination: Reactive Chlorine Emissions Inventory. *J. Geophys. Res. Atmos.* **1999**, *104*, 8347–8372. [[CrossRef](#)]
45. Wang, J.; Wood, R.; Jensen, M.P.; Chiu, J.C.; Liu, Y.; Lamer, K.; Desai, N.; Giangrande, S.E.; Knopf, D.A.; Kollias, P.; et al. Aerosol and Cloud Experiments in the Eastern North Atlantic (ACE-ENA). *Bull. Am. Meteorol. Soc.* **2021**, 1–51. [[CrossRef](#)]
46. Wang, Y.; Zheng, G.; Jensen, M.; Knopf, D.; Laskin, A.; Matthews, A.; Mechem, D.; Mei, F.; Moffet, R.; Sedlacek, A.; et al. Vertical Profiles of Trace Gas and Aerosol Properties over the Eastern North Atlantic: Variations with Season and Synoptic Condition. *Atmos. Chem. Phys. Discuss.* **2021**, *2021*, 1–39. [[CrossRef](#)]
47. Zawadowicz, M.A.; Suski, K.; Liu, J.; Pekour, M.; Fast, J.; Mei, F.; Sedlacek, A.J.; Springston, S.; Wang, Y.; Zaveri, R.A.; et al. Aircraft Measurements of Aerosol and Trace Gas Chemistry in the Eastern North Atlantic. *Atmos. Chem. Phys.* **2021**, *21*, 7983–8002. [[CrossRef](#)]
48. Zheng, G.J.; Wang, Y.; Aiken, A.C.; Gallo, F.; Jensen, M.P.; Kollias, P.; Kuang, C.G.; Luke, E.; Springston, S.; Uin, J.; et al. Marine Boundary Layer Aerosol in the Eastern North Atlantic: Seasonal Variations and Key Controlling Processes. *Atmos. Chem. Phys.* **2018**, *18*, 17615–17635. [[CrossRef](#)]
49. Wood, R.; Wyant, M.; Bretherton, C.S.; Remillard, J.; Kollias, P.; Fletcher, J.; Stemmler, J.; de Szoek, S.; Yuter, S.; Miller, M.; et al. Clouds, Aerosols, and Precipitation in the Marine Boundary Layer: An Arm Mobile Facility Deployment. *Bull. Am. Meteorol. Soc.* **2015**, *96*, 419–439. [[CrossRef](#)]
50. Parrish, D.D.; Trainer, M.; Holloway, J.S.; Yee, J.E.; Warshawsky, M.S.; Fehsenfeld, F.C.; Forbes, G.L.; Moody, J.L. Relationships Between Ozone and Carbon Monoxide at Surface Sites in the North Atlantic Region. *J. Geophys. Res. Atmos.* **1998**, *103*, 13357–13376. [[CrossRef](#)]
51. Raes, F.; Bates, T.; McGovern, F.; Van Liedekerke, M. The 2nd Aerosol Characterization Experiment (ACE-2): General Overview and Main Results. *Tellus Ser. B Chem. Phys. Meteorol.* **2000**, *52*, 111–125. [[CrossRef](#)]
52. Orsini, D.A.; Ma, Y.L.; Sullivan, A.; Sierau, B.; Baumann, K.; Weber, R.J. Refinements to the Particle-into-Liquid Sampler (PILS) for Ground and Airborne Measurements of Water Soluble Aerosol Composition. *Atmos. Environ.* **2003**, *37*, 1243–1259. [[CrossRef](#)]
53. Sorooshian, A.; Brechtel, F.J.; Ma, Y.; Weber, R.J.; Corless, A.; Flagan, R.C.; Seinfeld, J.H. Modeling and Characterization of a Particle-into-Liquid Sampler (PILS). *Aerosol Sci. Technol.* **2006**, *40*, 396–409. [[CrossRef](#)]
54. Marple, V.A.; Rubow, K.L.; Behm, S.M. A Microorifice Uniform Deposit Impactor (MOUDI): Description, Calibration, and Use. *Aerosol Sci. Technol.* **1991**, *14*, 434–446. [[CrossRef](#)]
55. Hennigan, C.J.; Izumi, J.; Sullivan, A.P.; Weber, R.J.; Nenes, A. A Critical Evaluation of Proxy Methods Used to Estimate the Acidity of Atmospheric Particles. *Atmos. Chem. Phys.* **2015**, *15*, 2775–2790. [[CrossRef](#)]
56. Fountoukis, C.; Nenes, A.; Sullivan, A.; Weber, R.; Van Reken, T.; Fischer, M.; Matias, E.; Moya, M.; Farmer, D.; Cohen, R.C. Thermodynamic Characterization of Mexico City Aerosol during MILAGRO 2006. *Atmos. Chem. Phys.* **2009**, *9*, 2141–2156. [[CrossRef](#)]
57. Bertram, A.K.; Martin, S.T.; Hanna, S.J.; Smith, M.L.; Bodsworth, A.; Chen, Q.; Kuwata, M.; Liu, A.; You, Y.; Zorn, S.R. Predicting the Relative Humidities of Liquid-Liquid Phase Separation, Efflorescence, and Deliquescence of Mixed Particles of Ammonium Sulfate, Organic Material, and Water Using the Organic-to-Sulfate Mass Ratio of the Particle and the Oxygen-to-Carbon Elemental Ratio of the Organic Component. *Atmos. Chem. Phys.* **2011**, *11*, 10995–11006. [[CrossRef](#)]
58. Malm, W.C.; Day, D.E. Estimates of Aerosol Species Scattering Characteristics as a Function of Relative Humidity. *Atmos. Environ.* **2001**, *35*, 2845–2860. [[CrossRef](#)]
59. Weber, R.J.; Guo, H.Y.; Russell, A.G.; Nenes, A. High Aerosol Acidity Despite Declining Atmospheric Sulfate Concentrations over the Past 15 Years. *Nat. Geosci.* **2016**, *9*, 282–285. [[CrossRef](#)]
60. Ding, J.; Zhao, P.S.; Su, J.; Dong, Q.; Du, X.; Zhang, Y.F. Aerosol pH and Its Driving Factors in Beijing. *Atmos. Chem. Phys.* **2019**, *19*, 7939–7954. [[CrossRef](#)]

61. Seinfeld, J.H.; Pandis, S.N. *Atmospheric Chemistry and Physics: From Air Pollution to Climate Change*, 3rd ed.; John Wiley & Sons: Hoboken, NJ, USA, 2016.
62. Whitby, K.T. The Physical Characteristics of Sulfur Aerosols. *Atmos. Environ.* **1978**, *12*, 135–159. [[CrossRef](#)]
63. Cruz, C.N.; Dassios, K.G.; Pandis, S.N. The Effect of Dioctyl Phthalate Films on the Ammonium Nitrate Aerosol Evaporation Rate. *Atmos. Environ.* **2000**, *34*, 3897–3905. [[CrossRef](#)]
64. Dassios, K.G.; Pandis, S.N. The Mass Accommodation Coefficient of Ammonium Nitrate Aerosol. *Atmos. Environ.* **1999**, *33*, 2993–3003. [[CrossRef](#)]
65. Dickson, A.G.; Goyet, C. *DOE: Handbook of Methods for the Analysis of the Various Parameters of the Carbon Dioxide System in Sea Water*; United States Department of Education: Washington, DC, USA, 1994.